ACS APPLIED NANO MATERIALS
Cite This: ACS Appl. Nano Mater. XXXX, XXX, XXX−XXX
Article
www.acsanm.org

Synthesis of Loose Nanodiamonds Containing Nitrogen-Vacancy Centers for Magnetic and Thermal Sensing

Alexandre Tallaire,*[,†,‡] Ovidiu Brinza,[‡] Mary De Feudis,[‡] Alban Ferrier,[†] Nadia Touati,[†] Laurent Binet,[†] Louis Nicolas,[§] Tom Delord,[§] Gabriel Hétet,[§] Tobias Herzig,[∥] Sébastien Pezzagna,[∥] Philippe Goldner,[†] and Jocelyn Achard[‡]

[†]Institut de Recherche de Chimie Paris, Chimie ParisTech, CNRS, PSL Research University, 11 rue Pierre et Marie Curie, 75231 Cedex 05 Paris, France

[‡]Laboratoire des Sciences des Procédés et des Matériaux, CNRS, Université Paris 13, Sorbonne Paris Cité, 93430 Villetaneuse, France

[§]Laboratoire Pierre Aigrain, Ecole Normale Supérieure, CNRS, PSL Research University, 24 rue Lhomond, 75231 Cedex 05 Paris, France

[∥]Department of Nuclear Solid-State Physics, University Leipzig, 04103 Leipzig, Germany

Supporting Information

ABSTRACT: The production of fluorescent nanodiamonds (NDs) with specific color centers and exhibiting a controlled size and purity represents an important challenge. In the context of quantum technologies they may indeed provide useful probes for magnetic or thermal sensing with extreme performance and biocompatibility. While detonation and grinding are the most used large-scale production methods, they do not allow for an accurate and flexible control over the defect content of the nanoparticles. In this work we report on the synthesis of loose NDs by high-power plasma chemical vapor deposition (CVD) without the need of a seeded substrate for nucleation. The as-grown NDs, dispersed in solution, exhibit high crystalline quality and low impurity background. A tunable amount of nitrogen-vacancy (NV) centers is introduced thanks to moderate N_2 additions during growth. Irradiation post-treatments using He^+ and H^+ ion beams followed by annealing are used to increase NV luminescence or create specific defects such as the helium-vacancy (HeV) center observed for the first time in a nanoscale material. Hydrogen-related impurities are, however, evidenced in electron paramagnetic resonance (EPR) spectroscopy and are likely to play a role in the preferential stabilization of the neutral charge state of the NV defect. Thanks to this synthesis approach, large-scale production of CVD NDs with a wide tunability of their chemical composition is achieved, paving the way to their use as a platform for exploring quantum sensing applications.

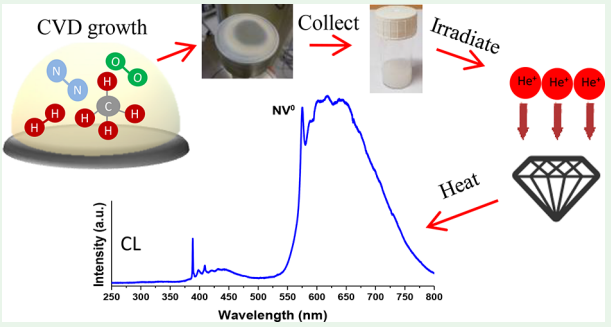

KEYWORDS: *diamond, nanoparticles, nitrogen-vacancy centers, plasma-assisted chemical vapor deposition, luminescent defects, ion bombardment*

INTRODUCTION

The unique properties of nanodiamonds (NDs) have sparked promising applications in a wide range of areas.[1] The ability to functionalize their surface with various chemical groups together with their biocompatibility has for example opened up new opportunities in medicine for drug delivery or biomarkers.[2−4] Recently, heavily boron-doped NDs[5] have been employed as local heating agents for the treatment of cancer cells.[6] NDs can also be integrated into lubricants or composites that benefit from improved mechanical and tribological properties while also providing better thermal conductivity.[7] The most sophisticated of these nanoparticles are produced with luminescent color centers such as the nitrogen vacancy (NV) or silicon vacancy (SiV)[8,9] that hold great promise for quantum technologies, in particular for sensing.[10,11] Indeed, the ability to manipulate and read out the NV spin state by monitoring its fluorescence under resonant MW excitation is at the basis of the development of magnetic probes[12,13] or local thermometry sensors[14] that offer extreme sensitivity, at room temperature, with nanoscale resolution. Although the spin properties of NVs in NDs remain well below that achieved in bulk diamonds (with coherence times (T_2) of the order of 1 μs rather than typically 300 μs for nonisotopically enriched single crystals),[15] their wide availability, low cost, and small dimensions are great assets for future applications. Producing NDs that have an appropriate

Received: July 24, 2019
Accepted: September 5, 2019
Published: September 5, 2019

DOI: 10.1021/acsanm.9b01395
ACS Appl. Nano Mater. XXXX, XXX, XXX−XXX

doping level, good crystallinity, high purity, photostability, and a controlled size, however, still remains an important challenge if one wants to address the desired quantum sensing applications.

So far there exists two main methods for synthesizing NDs in a relatively large amount: detonation and milling.[16] When explosives are detonated inside a closed vessel, high pressures and temperatures are reached at which diamond particles and other soot are deposited and later scrapped from the sidewalls. These so-called detonation nanodiamonds (DNDs) require additional time-consuming purification and separation steps to remove sp^2 phases and other contaminants.[17] Because explosives often contain nitrogen, NVs can be created, but the technique does not offer a great deal of control in the production of NDs with a tailored size and/or doping which is a serious limitation to their use in quantum technologies. Alternatively, through a top-down approach, grinding micrometric diamond grits or even single crystals can allow the production of milled nanodiamonds (MNDs) with a much higher crystalline quality. High-pressure, high-temperature (HPHT) type Ib diamonds are typically used as the starting powder.[18] They contain a significant amount of nitrogen as well as other metallic impurities from the melted bath used for synthesis although MNDs have also been produced from higher purity crystals.[19] Contamination from materials used for grinding (beads and mill walls) is unavoidable and requires acid cleaning. Mechanical damage induced by the process also drastically affects the properties of NV centers and induce unwanted inhomogeneous broadening.[20] More recently, the possibility to directly produce nano- or microdiamonds by HPHT without a metal catalyst by using carbonaceous precursors such as naphthalene ($C_{10}H_8$) is opening interesting prospects even though it still requires post-treatment steps to purify the material.[21]

Given the drawbacks and complexity of those production techniques, a few alternative approaches have been developed, such as laser ablation[22] or ultrasound cavitation.[23] Chemical vapor deposition (CVD) also appears as a suitable technique and has been used to produce isolated NDs containing NVs or more frequently SiVs. Such NDs are produced by heteroneous nucleation onto a seeded silicon wafer[24,25] or an Ir buffer layer[26] in a H_2/CH_4 plasma mixture at temperatures around 700−1000 °C. Although such particles exhibit good properties and sometimes single photon emission, the scalability of the process remains limited to small amounts. Contamination from the seeds or the semiconducting substrate that supports them is unavoidable. Strong adhesion of the particles onto the substrate also make it difficult to separate and disperse them in solution. Therefore, there still exists a need for new fabrication methods that can offer an accurate control over the doping level, isotopic purity, and coherent properties of loose fluorescent NDs to achieve efficient probes for magnetic or thermal sensing.

RESULTS AND DISCUSSION

In this paper we report on the direct synthesis of ND powders by plasma-assisted CVD under high power densities without the use of a seeded substrate. By tuning the growth conditions, fairly large amounts of NDs with a good crystallinity are reliably produced. In this process NV centers are created and controlled by intentionally adding moderate levels of nitrogen during growth while postgrowth irradiation treatments with helium ions or protons can enhance the fluorescence emission of the particles and create specific defects. Thanks to the accurate control of gas phase composition and growth conditions provided by the CVD technique, this approach provides a way to reliably mass-produce a material possessing higher purity or potentially isotopically enriched with improved properties as compared to conventional detonation or grinding processes.

The procedure used to synthesize the nanodiamonds by CVD is given in Scheme 1. ND powders were produced in a

Scheme 1. Procedure To Synthesize Nanodiamonds by Plasma-Assisted Chemical Vapor Deposition

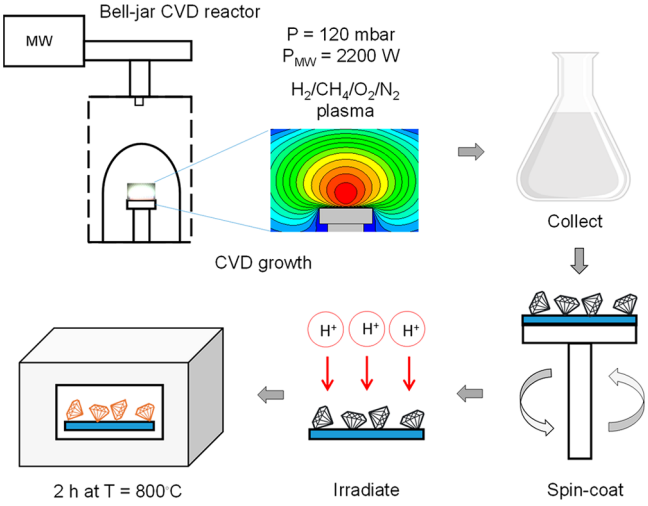

resonant cavity "bell-jar" type microwave reactor dedicated to the growth of high-purity diamond films and that operate under high power density (microwave power >2 kW) by using a $H_2/CH_4/O_2$ gas mixture. To assess the ability to produce luminescent defects inside the powders and to further tune their production, low amounts of N_2 from 0 to 250 ppm were added to the gas phase. The powdery deposit that builds up on the water-cooled molybdenum holder maintained at a temperature of around 450−550 °C is then washed in ethanol. The obtained suspension is grayish, in contrast to untreated DNDs or MNDs concentrated solutions that typically exhibit a black color (see the Supporting Information, Figure S1). This is a first indication that our material does contain a limited amount of graphitic phases. Eventually the nanodiamonds were sometimes submitted to an irradiation/annealing post-treatment.

Size and Crystallinity Assessment. The CVD NDs are agglomerated with round shape as seen in the scanning electron microscope (SEM) images of Figure 1a−d. The average size of the particles was statistically evaluated from the SEM images by measuring around 100 individual grains. It was found to be about 230 nm with a standard deviation of 100 nm for the undoped particles while it was estimated to 150 nm with a standard deviation of 70 nm for the 100 ppm of N_2-doped NDs (see Figure S2). Thus, NDs' size shows a moderate dependence with the doping level, with higher N_2 addition leading to slightly smaller particles. Unlike nitrogen-doped particles, undoped NDs had a more faceted and crystalline aspect. In addition, dynamic light scattering (DLS) analyses led to measured ND sizes ranging between 350 and 390 nm (see Figure S3), which is larger than what had been measured by SEM. However, DLS gives the hydrodynamic

DOI: 10.1021/acsanm.9b01395
ACS Appl. Nano Mater. XXXX, XXX, XXX−XXX

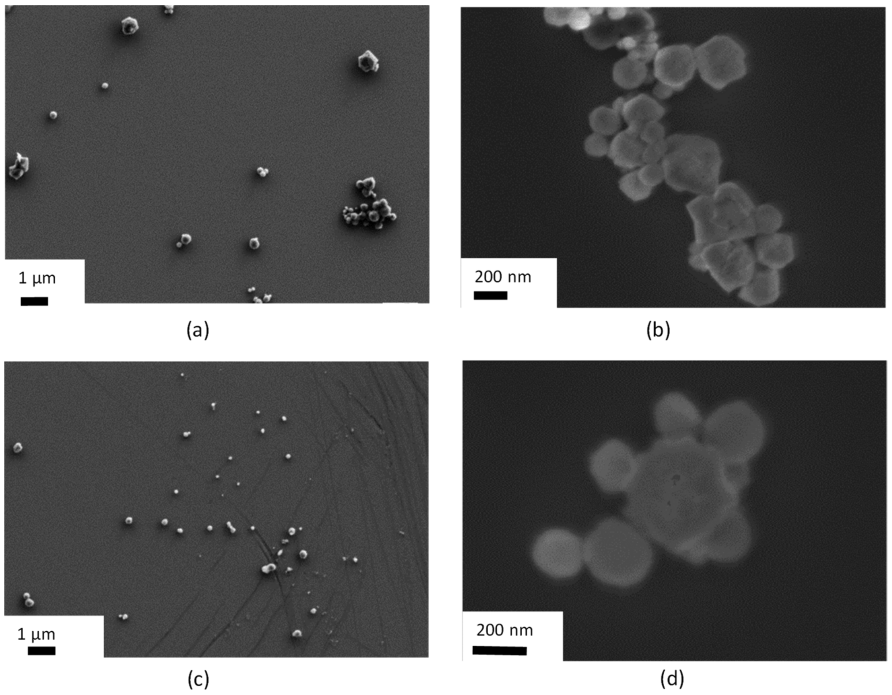

Figure 1. SEM images of CVD NDs grown with 0 (a, b) and 100 ppm of N_2 (b, c) that were drop-casted on a Si wafer.

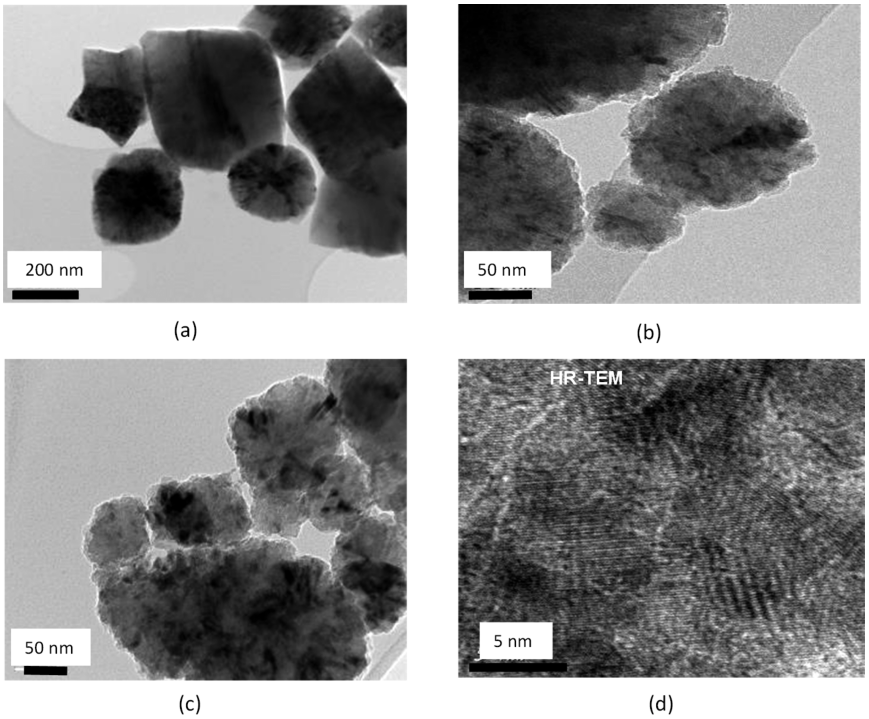

Figure 2. TEM images of CVD NDs grown with (a) 5 ppm of N_2 (b) 100 ppm of N_2, and (c) 250 ppm of N_2. (d) Lattice planes from small diamond grains can be identified on the high-resolution TEM image for the 250 ppm doped particles.

diameter which always tends to be overestimated compared to the real physical size. Although CVD ND's size is relatively high and dispersed for their use in bioapplications, changing the growth conditions was found to have an impact on their dimensions. Low power density conditions (1.7 kW MW power at a pressure of 100 mbar) mostly led to small diameter nanoparticles while high power density conditions (2.7 kW MW power at a pressure of 140 mbar) led to a larger amount of faceted grains (see Figure S4). This indicates that there potentially exists room for tuning the ND particles' dimensions by solely varying the plasma conditions. The use of post-treatments could also be implemented to reduce their dimensions and to filter them by size.[27]

To assess the crystallinity of the collected particles, transmission electron microscopy (TEM) images were acquired for NDs synthesized with 5, 100, and 250 ppm of N_2 (Figure 2). The particles were found to be composed of a crystalline core made of small grains with a size estimated to a

DOI: 10.1021/acsanm.9b01395
ACS Appl. Nano Mater. XXXX, XXX, XXX−XXX

few tens of nanometers (Figure 2d). The diamond phase in these polycrystalline particles is further evidenced by electron energy loss spectroscopy (EELS) analysis which shows a clear contribution from sp^3-coordinated carbon at 300 eV (σ orbitals) without any visible peak originating from π orbitals of graphite expected at 286 eV[28] (see Figure S5). The diamond particles are surrounded by an amorphous or graphitic shell that shows up as a wrinkled edge on the TEM images, but the nanocrystals did not contain a large amount of nondiamond phases.[29] Interestingly, we confirm that NDs synthesized with a low N_2 amount are more faceted with clearly defined and sharp edges. On the contrary, for high N_2 additions (250 ppm) the particles have a round shape without facets and a more developed graphitic shell. X-ray diffraction (XRD) of the CVD polycrystalline NDs presented in Figure S6 also shows characteristic peaks of the cubic diamond phase from which, based on Scherrer's formula, an average grain size of 18−20 nm can be extrapolated. This value is in agreement with the TEM observation. No peaks associated with the hexagonal form of diamond (lonsdaelite) were detected.[30]

Raman analysis was performed using a 473 nm laser as the excitation line for different NDs (Figure 3). DNDs show

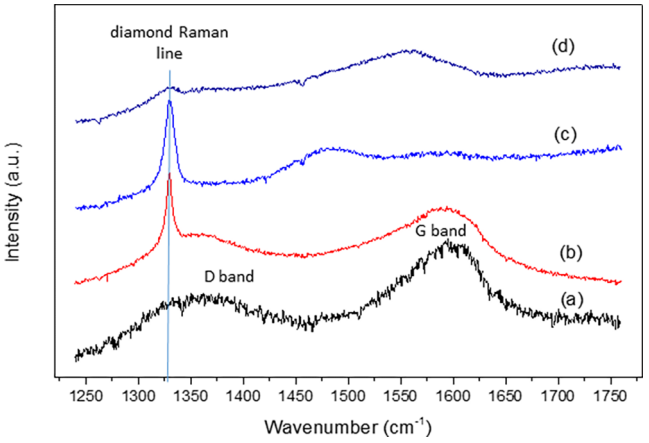

Figure 3. Raman spectroscopy of different NDs acquired with an excitation laser at 473 nm. (a) Detonation NDs, (b) milled NDs, (c) CVD NDs synthesized with 5 ppm of N_2 addition, and (d) CVD NDs synthesized with 250 ppm of N_2. Spectra are vertically shifted for clarity. The diamond Raman line and the graphite D and G bands are indicated.

amorphous and graphitic carbon D and G bands at 1380 and 1580 cm^{-1}, respectively, with no diamond peak at 1332 cm^{-1}. This is expected for untreated DNDs, and it is known that further purification by thermal or acid treatment would allow removing partially these sp^2 contributions.[29] MNDs, on the other hand, do show the same bands but with a pronounced diamond peak located at 1329.1 cm^{-1} with a full width at half maximum (fwhm) of 11 cm^{-1}. The shift toward lower wavenumbers of the diamond peak is expected for small dimensions particles. Our CVD-grown NDs show nearly no visible graphitic bands, and particularly the 5 ppm of N_2-doped ones exhibit an intense diamond Raman peak at 1329.7 cm^{-1} with a fwhm of 13 cm^{-1}. An additional band at 1470 cm^{-1} has an unclear origin but could be related to *trans*-polyacetylene[31] or amorphous carbon.[32] On the contrary, CVD NDs produced with the highest N_2 addition (250 ppm) exhibit sp^2 contributions and a much reduced diamond peak which confirms their lower crystalline quality, in agreement with previous TEM observations. This analysis supports the high crystalline quality of our synthetic material.

Luminescence Properties. Photoluminescence (PL) and Raman spectroscopy were also performed by using a 532 nm excitation laser for different types of NDs (see Figure S7). CVD NDs show many unattributed luminescence peaks that could be related to the presence of adsorbed organic species at the surface of the dispersed particles or luminescence stemming from grain boundaries.[33] Surface treatments of the nanodiamonds in acidic or basic solutions associated with thermal annealing could be studied in the near future to reduce this background luminescence. However, emission from NV centers in these as-grown CVD NDs cannot be easily evidenced by optical excitation, even with a green laser, possibly because of quenching or their low density with respect to other defects or impurities. In fact, it has been recently reported that for highly nitrogen doped diamonds the proximity of NV^- and N^+ pairs may also lead to quenching of the photoluminescence.[34]

We turned to cathodoluminescence (CL) spectroscopy performed at 110 K to identify luminescent defects in our CVD NDs synthesized with various nitrogen doping (Figure 4a). NV^0 emission at 575 nm clearly appears as soon as 5 ppm

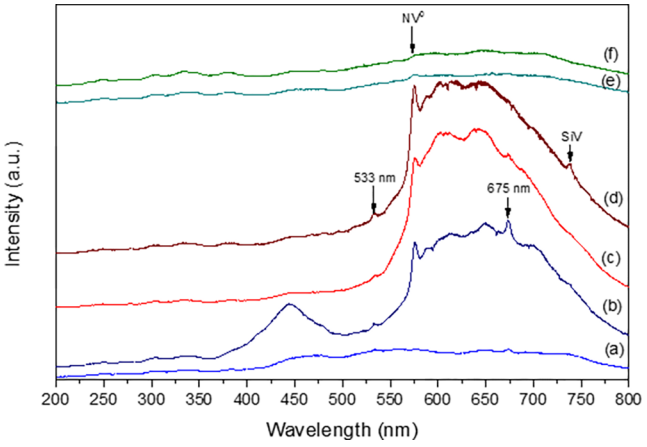

Figure 4. Low-temperature (110 K) CL spectroscopy of CVD NDs synthesized with different amounts of nitrogen: (a) 0, (b) 5, (c) 20, (d) 50, (e) 100, and (f) 250 ppm. The main emissions are identified, and spectra are vertically shifted for clarity.

of N_2 is added to the gas phase. It is accompanied by another peak at 533 nm that is known to be nitrogen related.[35,36] We note that NV^- luminescence expected at 637 nm is not active in CL and is thus not visible here.[37] NV^0 emission completely disappears for 250 ppm of N_2, and the spectrum shows lower overall emission. Another luminescence peak at 675 nm which has yet not been attributed to any specific defect is particularly strong for lower doping. In some cases the silicon-vacancy (SiV^-) peak at 737 nm appears (Figure 4d) although there exists substantial variation in intensity depending on the particle on which the measurement is performed within the same ND batch, independently of doping. In general, SiV^- emission is fairly scarce, indicating a low contamination from Si impurities since our deposition is substrateless. Si impurities may, however, come from the walls of the quartz bell-jar reactor used for synthesis. A broad blue emission around 450 nm (Figure 4b) known as band A and related to extended defects such as dislocations in diamond also appears with

DOI: 10.1021/acsanm.9b01395
ACS Appl. Nano Mater. XXXX, XXX, XXX−XXX

substantial variation depending on the considered particle.[38] From the relative CL intensity, it is observed that NV doping level can be controlled with moderate N_2 additions during synthesis (<50 ppm). The produced particles are rather emissive with only limited background fluorescence and silicon contamination. Additional comparative CL results were obtained at room temperature on other types of NDs (see Figure S8), including commercial irradiated detonation NDs and milled NDs. Our CVD-grown material shows a comparable emission to that of fluorescent detonation NDs even though we used no irradiation treatment.

Irradiation of Nanodiamonds. Post-treatments are commonly used to boost fluorescence emission of NDs. Irradiation with ions, electrons, or proton beams[39] associated with HPHT annealing[40] indeed provides a way to partially convert substitutional nitrogen into color centers through creation and diffusion of vacancies. To further tailor luminescent defects production and demonstrate the potential of our CVD NDs, we thus performed different irradiation treatments.[10,41] First, we used a He^+ ion beam from a standard ion etcher at 10 keV for 2 s with a rather high dose of about 10^{13} ions cm^{-2}. The main advantage of this type of irradiation system is that given the relatively high mass of the incident ions, low energies and thus compact laboratory equipment can be used. We calculated a penetration depth of about 50 nm which would lead to the creation of vacancies with a density around 4×10^{21} cm^{-3} (i.e., slightly below the graphitization threshold of 10^{22} cm^{-2}). The irradiated NDs were then annealed under vacuum (10^{-6} mbar) for 2 h at 750 °C followed by 2 h at 850 °C to allow for vacancies to diffuse. Room temperature CL analysis was performed after irradiation and after annealing for the 5 ppm of N_2-doped CVD NDs (Figure 5). Following irradiation the well-known radiation

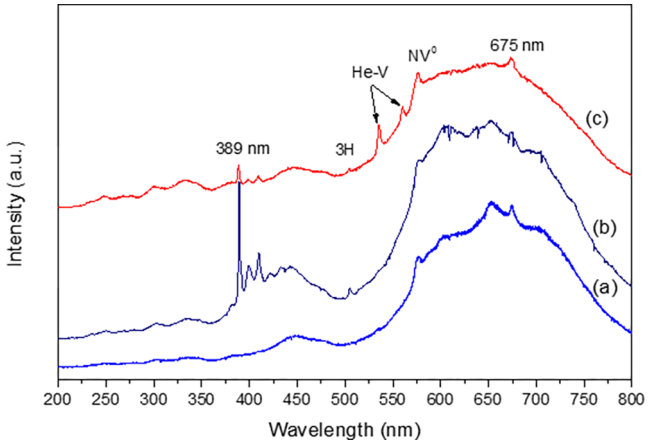

Figure 5. Room temperature CL of 5 ppm of N_2-doped CVD NDs (a) as-grown, (b) after He^+ irradiation at 10 keV and 10^{13} ions cm^{-2}, and (c) after annealing. Spectra were vertically shifted for clarity. Different color centers are identified.

damage center with a zero phonon line (ZPL) at 389 nm and clear phonon side bands[42] appeared. It likely involves nitrogen and interstitial atoms, indicating that irradiation successfully modified the crystal structure. The 3H center (503.5 nm), a negatively charged defect sometimes found in N-containing diamonds upon irradiation and attributed to double interstitials, was also detected.[43] After annealing, the intensity of the 389 nm center strongly decreased. SiV^- emission, expected at 737 nm, was not enhanced by the irradiation underlying again that Si is a minor contaminant. NV^0 intensity only slightly increased following He^+ irradiation/annealing although the effect was not easily quantifiable by CL. This is possibly due to the rather high dose received by the sample in the ion etching system used for the irradiation. One can also note that the luminescence at 675 nm remained mostly unchanged throughout the irradiation and annealing treatments. Interestingly, two new lines appeared at around 536 and 560 nm. They have been recently reported in bulk diamond crystals after high-energy He^+ implantation and have been tentatively assigned to helium-vacancy (HeV) centers.[44] This is the first time that these centers are detected in irradiated NDs. This is encouraging and indicates that specific color centers can be successfully created in this material when adapted irradiation treatments are used.

To further tune NV emission, we then irradiated NDs with a dedicated 80 keV collimated proton beam (H^+) from a more bulky implantation system which allows for accurate control of the dose in the range 10^{13} to 3×10^{15} cm^{-2}.[45,46] Indeed, because of the lower mass of H^+ ions, fewer vacancies are created per incident particle as compared to He^+. The irradiated NDs were then annealed under vacuum for 2 h at 930 °C before being analyzed by CL and PL. Results of the CL analysis are presented in Figure 6 for different proton fluencies.

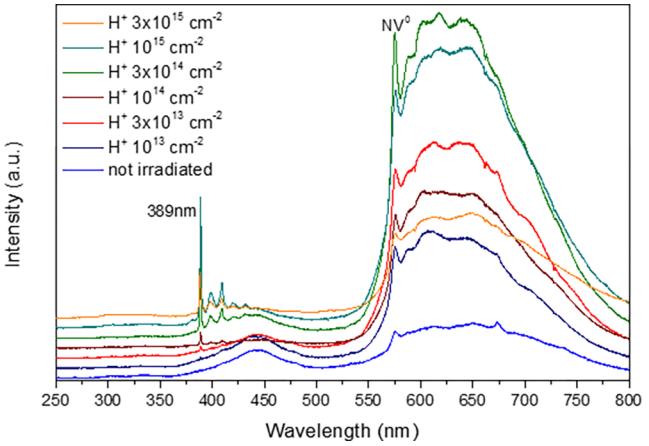

Figure 6. Room temperature CL of 5 ppm of N_2-doped CVD NDs after different proton irradiation at doses ranging from 10^{13} to 3×10^{15} cm^{-2} at an energy of 80 keV and subsequent thermal annealing. Spectra were vertically shifted for clarity.

It is striking that the luminescence intensity of NV^0 emission at 575 nm strongly increases with the irradiation dose. It reaches a maximum at 3×10^{14} cm^{-2}, starts to decrease at 10^{15} cm^{-2}, and finally collapses at an irradiation dose of 3×10^{15} cm^{-2} (orange curve of Figure 6). This is consistent with the appearance of a dark spot on the sample for the highest doses. A similar trend appears for the radiation-damage center at 389 nm.[47] The 675 nm color center did not seem to be enhanced by the treatment, indicating that it is probably not associated with vacancies. Unlike irradiation with the He^+ ion beam, we here managed to get into a regime where vacancies creation is precisely tuned below the graphitization threshold, leading to an obvious improvement of NV luminescence. Treatment with a high-energy electron beam (of a few MeV) will also be attempted to generate vacancies more uniformly and without unwanted contamination for He or H atoms. Indeed, this

DOI: 10.1021/acsanm.9b01395
ACS Appl. Nano Mater. XXXX, XXX, XXX−XXX

approach is known to lead to improved optical properties although it requires a bulky irradiation equipment that was not available in this study.

Additionally, we performed room temperature PL measurements on the proton-irradiated NDs using a 473 nm excitation line (Figure 7). A clear signature from NV^0 centers was found,

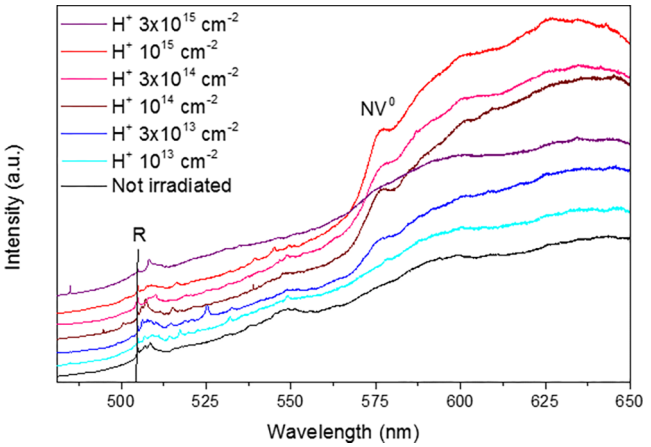

Figure 7. PL spectroscopy of CVD NDs irradiated with different proton doses by using a 473 nm excitation laser. The position of the diamond Raman peak is identified by a vertical line and labeled "R". Spectra were vertically shifted for clarity.

the intensity of which increased with the irradiation dose up to 10^{15} cm^{-2}, after which it started to decrease. This is consistent with the previous CL results. The negative charge state of the NV center expected at 637 nm was, however, not clearly visible and overlapped with other sharp peaks possibly due to defects and impurities at grain boundaries that might quench the emission.[33] A relatively low NV^- density together with unoptimized excitation wavelength also contributed to limit the emission efficiency.[34] Nevertheless, we also observe that the unattributed luminescence peak observed previously is less evident due to the higher contribution from NV centers in such irradiated diamonds. Observation under the 235 nm UV light from a DiamondView instrument confirmed that the red glow was enhanced by the proton irradiation treatment which increased the luminescence from NV centers (see Figure S9). Further tuning of the growth conditions or post-treatment procedure might allow stabilizing the negative charge state of the defect and increasing the potential of this material for quantum technologies applications.[48] Nevertheless, we assessed PL lifetime of the brightest CVD NDs that were irradiated with a proton fluence of 3×10^{14} cm^{-2} (Figure 8a). The fluorescence decay presented in Figure 8b was filtered in the 550−650 nm range which corresponds to NV^0 center emission. After deconvolution by the pulsed response of the system (pulsed laser and avalanche photodiode), we were able to fit the curves by a double exponential with lifetimes τ_1 of 1.4 ± 0.5 ns and τ_2 of 12.8 ± 0.5 ns. The shorter decay lifetime has been attributed to quenching by surface-related defects,[49] while the longer lifetime is consistent with typical values reported for NV^0 centers in nanodiamonds.[50]

Impurity Analysis. To assess the presence of defects and impurities in our NDs, which could potentially quench NV^- emission or reduce their coherence properties, we performed continuous wave electron paramagnetic resonance (EPR) spectroscopy at room temperature on nonirradiated as-grown NDs. In Figure 9a, the EPR spectra obtained in the X-band for our CVD NDs grown with different N_2 amounts are presented. They consist of a broad central line with a g factor of 2.0026 and additional weaker shoulders particularly visible for the highest doping level that can be attributed to unpaired electrons with a $S = 1/2$ state. We note that we were not able to detect EPR signal from NV^- centers in the half-field region as reported in irradiated and annealed fluorescent diamonds.[51] This is probably due to the relatively low concentration of NV^- centers in our material. In addition, no EPR signal attributed to P1 centers (isolated substitutional nitrogen) with its characteristic hyperfine structure could be evidenced.[52] It is indeed known that due to interaction of P1 with surface defects, the hyperfine structure may disappear for NDs with a small grain size (<150 nm)[53] unless specific annealing post-treatments are used.[54]

To clarify the origin of the signal observed for our NDs, we performed additional continuous-wave EPR measurements in the Q-band for a sample with 20 ppm of N_2 doping in the gas phase as shown in Figure 9b. It appears that the distance between the satellites increases with frequency. This microwave frequency dependence of the line shape is characteristic of the H1 defect center, attributed to a hydrogen-vacancy-like (HV) complex.[55,56] This defect is commonly found in CVD

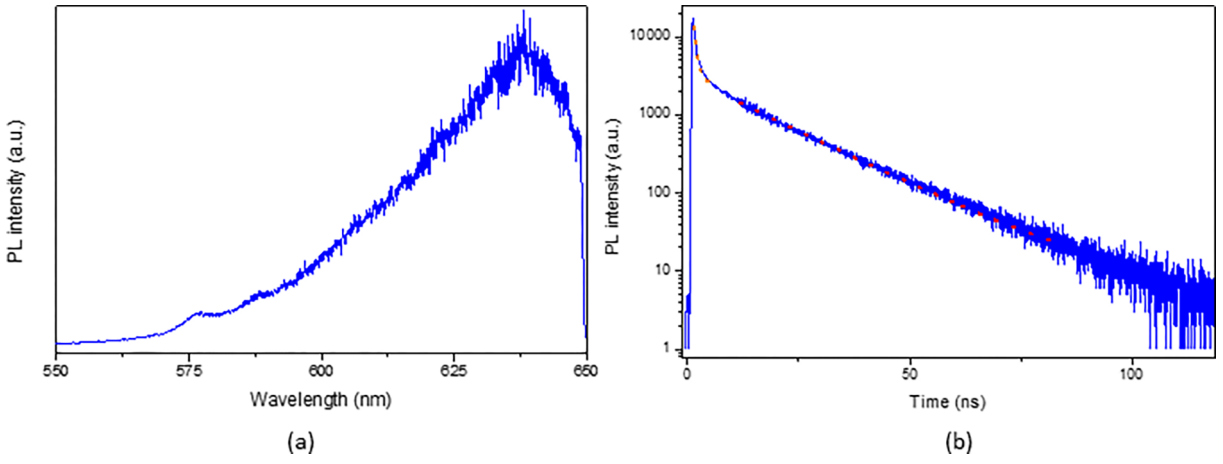

Figure 8. (a) PL emission and (b) corresponding PL lifetime in the range 550−650 nm for NDs irradiated with a proton fluence of 3×10^{14} cm^{-2}. The curve can be fitted by two exponentials that are displayed with dashed lines.

DOI: 10.1021/acsanm.9b01395
ACS Appl. Nano Mater. XXXX, XXX, XXX−XXX

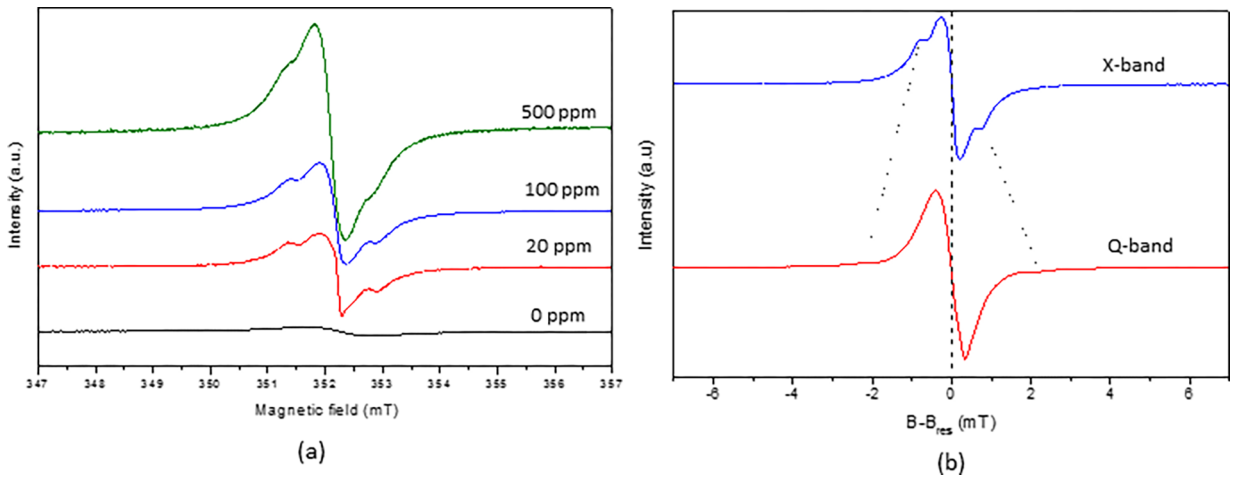

Figure 9. (a) Room temperature X-band EPR spectra of CVD NDs grown with 0, 20, 100, and 500 ppm of N_2 added to the gas phase. NDs were as grown and not irradiated prior to measurement. Spectra were normalized to the mass of the powder analyzed. (b) X-band and Q-band EPR spectra of CVD NDs grown with 20 ppm of added N_2 to the gas phase as a function of the magnetic shift from the resonance field B_{res}. Spectra were vertically shifted.

diamonds grown under H_2-rich conditions[57,58] where they are believed to be mostly located at grain boundaries or intergranular material rather than in the bulk of the crystal. We note that the measured NDs were as-grown, and thus hydrogen contamination does not come from proton irradiation treatment. We then compared the doubly integrated EPR signal of this broad line acquired for different ND samples with that of DPPH free radicals crystals (α-diphenyl-β-picrylhydrazyl with a spin density of 10^{17} g^{-1}). The calculated spin density reported in Table 1 represents the total amount of

Table 1. Spin Density Calculated from the Integration of the Central Broad Line in EPR

N_2 doping in the gas phase	spin density (g^{-1})	spin density (ppm)
0	2.8×10^{18}	55 ± 10
20	1.4×10^{19}	270 ± 10
100	1.6×10^{19}	320 ± 10
500	2.9×10^{19}	580 ± 10

defects having a spin 1/2 that include the H1 center. The order of magnitude is consistent with that reported for DNDs.[59] Interestingly, when N_2 was added to the gas phase during synthesis, the spin density increased almost linearly. The more distorted polycrystalline structure of NDs grown with intentional addition of N_2, as observed in TEM, could explain the higher detected amount of H1 centers. The presence of these H-related defects is likely to play a role in passivating or quenching NV luminescence, and strategies allowing reducing their appearance would be needed.

NDs Synthesis and Color Center Creation Mechanisms. The main route for NDs production using our high power density CVD process is believed to be direct homogeneous nucleation in the gas phase and agglomeration onto the cold holder by thermophoresis. In fact, in the core of the plasma, temperatures as high as 3000 K are expected, and thermal dissociation of the chemical species is promoted.[60] If the surface temperature of a substrate is maintained at 700 °C or more, a continuous polycrystalline diamond film grows. This leads to the conventional seeded diamond growth on a substrate. In contrast, in our process, low surface temperatures (<500 °C) and the absence of seeding do not allow for significant heterogeneous nucleation and columnar growth to occur. The low reactivity of the cold molybdenum holder ensures that agglomerated particles do not react at the surface while atomic hydrogen and oxygen produced in a large amount in the high power plasma help stabilizing the diamond phase by etching away any unwanted sp^2 phases that may be formed. The small size of nucleated diamond particles also favors their stability in the gas phase.[61] The proposed mechanism is supported by a recent study from Kumar et al.,[62] who have shown that NDs down to 3 nm in size can be produced at low surface temperature and at atmospheric pressure in an Ar/H_2/ethanol postdischarge using a dedicated microplasma system. Despite the different setups, high plasma densities might be expected locally in a similar way to those reached at a larger scale in our plasma-assisted CVD reactor. Nucleation of a low amount of diamond particles was also reported in a dusty low-pressure, low-power microwave plasma[63] or in the presence of diborane.[64] In our work, thanks to the use of high plasma densities and an appropriate gas mixture, the synthesis of relatively large quantities of loose NDs at the wafer scale is possible at a rate of typically 1 mg/h.

In addition, we demonstrate that nitrogen doping in the produced NDs can be adjusted by adding N_2 in the tens of ppm range to the gas phase. The use of high power densities enhances the dissociation of the very stable N_2 molecule and is favorable to higher doping efficiency even under low added amounts.[36] However, in a similar way to what is observed with a single crystal diamond, the presence of too high N_2 levels is detrimental to the crystalline quality and leads to the appearance of more defective round-shaped crystals with significantly enhanced graphitic phases and grain boundaries. This sets the upper limit for N_2 additions to about 100 ppm in our conditions, which is slightly lower than the maximum amount acceptable for single crystal diamond growth.[65] An unambiguous signature from NV^0 centers is visible in CL and indicates that there exists an optimum for a few tens of ppm of added N_2 to reach a maximum doping level. On the other hand, PL emission is not easily detected for NV^0 and is almost absent for NV^-. NV emission in PL is likely to be quenched by other defects and impurities present in the NDs, particularly at their grain boundaries. Indeed, EPR analysis shows that a

DOI: 10.1021/acsanm.9b01395
ACS Appl. Nano Mater. XXXX, XXX, XXX−XXX

significant level of hydrogen is incorporated, leading to the appearance of the well-known H1 center. Hydrogen incorporation could play a passivating role on NV^- or may quench their emission although more investigation would be needed. Nevertheless, further improvement of the luminescent properties of our material would probably require that the amount of hydrogen incorporation and/or the presence of grain boundaries are reduced.

Irradiation post-treatments with He^+ or H^+ ions followed by high-temperature annealing is also demonstrated to create specific emitters such as the HeV center or to boost the overall NV fluorescence. These post-treatments may require more optimization to push further the optical properties of the doped color centers. In addition, they could be associated with chemical treatments that aim at modifying the NDs' surface termination, which is naturally H-terminated after growth, and stabilizing the negative charge state of the NV center. In fact, it has recently been shown that specially prepared OH-terminated detonation NDs possess improved optical properties.[66]

CONCLUSIONS

In summary, we demonstrated a new flexible approach to synthesize loose NDs by homogeneous nucleation in a high power density plasma CVD reactor without the need of a seeded substrate which could open interesting perspectives toward the development of magnetic or thermal sensing probes. The ∼200 nm NDs consisted of agglomerated polycrystalline particles with a grain size of about 18−20 nm that were easily collected. Raman, EELS, and XRD measurements confirmed their high crystalline quality without any apparent contribution from sp^2 phases. We were able to create a controlled amount of NV centers in these NDs with moderate additions of N_2 during synthesis (<50 ppm). Too high levels of N_2 were detrimental to both the crystalline quality and NV emission. He^+ irradiation at 10 keV and a fluence of 10^{13} cm^{-2} allowed modifying the nature and amount of defects, leading to the creation of HeV centers for the first time in a nanoscale material. With more controlled proton irradiations at 80 keV (10^{15} cm^{-2}) we achieved an enhanced NV emission. Nevertheless, PL from negatively charged NV^- centers in as-grown NDs remained limited and is likely quenched by other defects and impurities. EPR analysis showed that a significant amount of hydrogen was incorporated, potentially playing a role in this passivation or quenching mechanism. Limiting the presence of grain boundaries where this hydrogen is mostly located will be key to improving this issue.

It is believed that by further tuning the CVD growth conditions, the size, chemical composition, isotopic content ($^{12}C/^{13}C$ ratio), and properties of NDs produced by this technique could be varied to a great extent, which would be challenging or even unreachable with other production methods. CVD NDs are also naturally hydrogen-terminated which is desirable for many applications.[67,68] The implementation of post-treatments that have been widely developed for DNDs and MNDs such as functionalization, centrifugation, or electron irradiation at a larger scale could provide a way to create batches of fluorescent nanoparticles. Loose and dispersed NDs produced by this approach could thus be established as a useful platform for quantum technologies in particular for sensing or as fluorescent markers in bioapplications.

METHODS

ND Synthesis. NDs were grown in a plasma-assisted quartz bell-jar reactor (BJS-150) codeveloped between the LSPM laboratory and Plassys Company. The system uses microwaves at 2.45 GHz in a resonant cavity design to couple power to the generated plasma. Fairly high pressures and microwave powers (120 mbar/2.2 kW) were used with a typical gas mixture of $H_2/CH_4/O_2$ (93.2/6/0.8) and a total gas flow of 500 sccm. A clean but already plasma exposed 2 in. molybdenum holder was placed onto a water-cooled stage so that its temperature was maintained in the range 450−500 °C as measured by a dual-wavelength pyrometer. NDs agglomerated on the holder were flushed away by ethanol and collected.

Structural Characterization. NDs were spin-coated onto a silicon wafer for SEM analysis in a ZEISS Ultratorr field effect gun (FEG) system. TEM observation was performed in a JEOL 200 kV microscope with the NDs suspension drop-casted onto a carbon TEM grid. XRD analysis was performed in a PANALYTICAL XPERT-Pro diffractometer.

Luminescence Assessment. PL and Raman analysis were performed at room temperature in a dedicated micro-Raman Renishaw InVia apparatus using excitation with diode lasers emitting at 532 or 473 nm and 1200 or 2400 grooves gratings, respectively.

For the CL measurement, a liquid nitrogen cooled stage was used to lower down the temperature to about 110 K. The electron beam of a ZEISS EVOMA15 SEM system at 10 keV and 20 nA was used to create the excitation. Luminescence was collected with a parabolic mirror and analyzed in a spectrometer equipped with a 600 grooves grating and a slit size of 100 μm (Horiba HCLUE).

PL images were also acquired using a DiamondView equipment. This setup uses UV light at near the diamond band gap (225 nm) to excite luminescence while an image of the sample is simultaneously recorded.

PL lifetime measurements were performed using a home-built confocal microscope with a numerical aperture of 0.4. The sample was excited thanks to a 520 nm laser diode (PicoQuant LDH-D-C-520) with a pulse length of 480 ps. PL was collected in the range 550−650 nm by using a filter and coupled to a monomode fiber before being sent to an avalanche photodiode (SPCM-AQRH-15 Excelitas Technologies).

Irradiation. For the irradiation experiments the suspension of NDs in ethanol was dried onto a silicon wafer before being exposed to the ion beam. He^+ irradiation was performed by using a standard ion etcher (GATAN PIPS) at a beam current of 50 μA, a 10 keV energy for 2 s, and a beam size of 10 mm. H^+ irradiation was performed in a homemade dedicated accelerator at 80 keV for doses ranging from 10^{13} to 3×10^{15} cm^{-2} and a spot size of 1.3 mm. Following implantation, annealing was performed in a vacuum furnace at a base pressure of 10^{-6} mbar for 2 h at 930 °C for the H^+ irradiation and 2 h at 750 °C followed by 2 h at 850 °C for the He^+ irradiation experiment.

EPR Analysis. Continuous wave electron paramagnetic resonance experiments were performed at X-band operating at 9.87 GHz and Q-band operating at 34 GHz in a Bruker ELEXSYS E500 spectrometer. The samples were weighted and inserted in a quartz tube. The spectra were recorded under nonsaturated conditions using a SHQE cavity. A DPPH powder was used to estimate the spin number in the sample analyzed. DPPH EPR spectra were performed with the same temperature and acquisition parameters as the samples.

ASSOCIATED CONTENT

Supporting Information

The Supporting Information is available free of charge on the ACS Publications website at DOI: 10.1021/acsanm.9b01395.

Images of the gray CVD NDs suspensions compared to black commercial nanodiamonds; size distribution of NDs measured from the SEM pictures and by DLS; SEM images of CVD-NDs grown under various plasma conditions and exhibiting different grain sizes; EELS

DOI: 10.1021/acsanm.9b01395
ACS Appl. Nano Mater. XXXX, XXX, XXX−XXX

spectra acquired in the TEM microscope and exhibiting the characteristic signature from sp^3 carbon; X-ray diffraction spectrum of CVD NDs showing the cubic lattice planes of diamond. PL and CL spectra of as-grown NDs with various doping compared with commercial particles; DiamondView PL images of the irradiated NDs (PDF)

AUTHOR INFORMATION

Corresponding Author

*E-mail alexandre.tallaire@chimie-paristech.fr.

ORCID

Alexandre Tallaire: 0000-0002-0663-6662

Notes

The authors declare no competing financial interest.

ACKNOWLEDGMENTS

This project has received funding from the European Union's research and innovation program under grant agreement no. 820394 (ASTERIQS) as well as by the international ERA-NET on Quantum Technologies no. ANR-18-QUAN-0008-03 (MICROSENS). It has been cofunded by Ile-de-France region in the framework of DIM-SIRTEQ and the French Labex SEAM (Sciences and Engineering for Advanced Materials and devices) supported by CGI (Commissariat Général à l'Investissement).

REFERENCES

(1) Mochalin, V. N.; Shenderova, O. A.; Ho, D.; Gogotsi, Y. The properties and applications of nanodiamonds. *Nat. Nanotechnol.* **2012**, *7*, 11−23.

(2) Ho, D. Beyond the Sparkle: The Impact of Nanodiamonds as Biolabeling and Therapeutic Agents. *ACS Nano* **2009**, *3*, 3825−3829.

(3) Wu, Y.; Jelezko, F.; Plenio, M. B.; Weil, T. Diamond Quantum Devices in Biology. *Angew. Chem., Int. Ed.* **2016**, *55*, 6586−6598.

(4) Chipaux, M.; van der Laan, K. J.; Hemelaar, S. R.; Hasani, M.; Zheng, T.; Schirhagl, R. Nanodiamonds and Their Applications in Cells. *Small* **2018**, *14*, 1704263.

(5) Heyer, S.; Janssen, W.; Turner, S.; Lu, Y.-G.; Yeap, W. S.; Verbeeck, J.; Haenen, K.; Krueger, A. Toward Deep Blue Nano Hope Diamonds: Heavily Boron-Doped Diamond Nanoparticles. *ACS Nano* **2014**, *8*, 5757−5764.

(6) Vervald, A. M.; Burikov, S. A.; Vlasov, I. I.; Ekimov, E. A.; Shenderova, O. A.; Dolenko, T. A. Boron-doped nanodiamonds as possible agents for local hyperthermia. *Laser Phys. Lett.* **2017**, *14*, 045702.

(7) Mizuuchi, K.; Inoue, K.; Agari, Y.; Morisada, Y.; Sugioka, M.; Tanaka, M.; Takeuchi, T.; Kawahara, M.; Makino, Y. Thermal conductivity of diamond particle dispersed aluminum matrix composites fabricated in solid−liquid co-existent state by SPS. *Composites, Part B* **2011**, *42*, 1029−1034.

(8) Jantzen, U.; Kurz, A. B.; Rudnicki, D. S.; Schäfermeier, C.; Jahnke, K. D.; Andersen, U. L.; Davydov, V. A.; Agafonov, V. N.; Kubanek, A.; Rogers, L. J.; Jelezko, F. Nanodiamonds carrying silicon-vacancy quantum emitters with almost lifetime-limited linewidths. *New J. Phys.* **2016**, *18*, 073036.

(9) Ralchenko, V. G.; Sedov, V. S.; Martyanov, A. K.; Bolshakov, A. P.; Boldyrev, K. N.; Krivobok, V. S.; Nikolaev, S. N.; Bolshedvorskii, S. V.; Rubinas, O. R.; Akimov, A. V.; Khomich, A. A.; Bushuev, E. V.; Khmelnitsky, R. A.; Konov, V. I. Monoisotopic Ensembles of Silicon-Vacancy Color Centers with Narrow-Line Luminescence in Homoepitaxial Diamond Layers Grown in H2−CH4−[x]SiH4 Gas Mixtures (x = 28, 29, 30). *ACS Photonics* **2019**, *6* (1), 66−72.

(10) Chang, Y.-R.; Lee, H.-Y.; Chen, K.; Chang, C.-C.; Tsai, D.-S.; Fu, C.-C.; Lim, T.-S.; Tzeng, Y.-K.; Fang, C.-Y.; Han, C.-C.; Chang, H.-C.; Fann, W. Mass production and dynamic imaging of fluorescent nanodiamonds. *Nat. Nanotechnol.* **2008**, *3*, 284−288.

(11) Tisler, J.; Balasubramanian, G.; Naydenov, B.; Kolesov, R.; Grotz, B.; Reuter, R.; Boudou, J.-P.; Curmi, P. A.; Sennour, M.; Thorel, A.; Börsch, M.; Aulenbacher, K.; Erdmann, R.; Hemmer, P. R.; Jelezko, F.; Wrachtrup, J. Fluorescence and Spin Properties of Defects in Single Digit Nanodiamonds. *ACS Nano* **2009**, *3*, 1959−1965.

(12) Rondin, L.; Tetienne, J.-P.; Hingant, T.; Roch, J.-F.; Maletinsky, P.; Jacques, V. Magnetometry with nitrogen-vacancy defects in diamond. *Rep. Prog. Phys.* **2014**, *77*, 056503.

(13) Tetienne, J. P.; Hingant, T.; Rondin, L.; Cavaillès, A.; Mayer, L.; Dantelle, G.; Gacoin, T.; Wrachtrup, J.; Roch, J. F.; Jacques, V. Spin relaxometry of single nitrogen-vacancy defects in diamond nanocrystals for magnetic noise sensing. *Phys. Rev. B: Condens. Matter Mater. Phys.* **2013**, *87*, 235436.

(14) Neumann, P.; Jakobi, I.; Dolde, F.; Burk, C.; Reuter, R.; Waldherr, G.; Honert, J.; Wolf, T.; Brunner, A.; Shim, J. H.; Suter, D.; Sumiya, H.; Isoya, J.; Wrachtrup, J. High-Precision Nanoscale Temperature Sensing Using Single Defects in Diamond. *Nano Lett.* **2013**, *13*, 2738−2742.

(15) Knowles, H. S.; Kara, D. M.; Atatüre, M. Observing bulk diamond spin coherence in high-purity nanodiamonds. *Nat. Mater.* **2014**, *13*, 21−25.

(16) Nunn, N.; Torelli, M.; McGuire, G.; Shenderova, O. Nanodiamond: A high impact nanomaterial. *Curr. Opin. Solid State Mater. Sci.* **2017**, *21*, 1−9.

(17) Liang, Y.; Ozawa, M.; Krueger, A. A General Procedure to Functionalize Agglomerating Nanoparticles Demonstrated on Nanodiamond. *ACS Nano* **2009**, *3*, 2288−2296.

(18) Mahfouz, R.; Floyd, D. L.; Peng, W.; Choy, J. T.; Loncar, M.; Bakr, O. M. Size-controlled fluorescent nanodiamonds: a facile method of fabrication and color-center counting. *Nanoscale* **2013**, *5*, 11776−11782.

(19) Neu, E.; Arend, C.; Gross, E.; Guldner, F.; Hepp, C.; Steinmetz, D.; Zscherpel, E.; Ghodbane, S.; Sternschulte, H.; Steinmüller-Nethl, D.; Liang, Y.; Krueger, A.; Becher, C. Narrowband fluorescent nanodiamonds produced from chemical vapor deposition films. *Appl. Phys. Lett.* **2011**, *98*, 243107.

(20) Rosenzweig, Y.; Schlussel, Y.; Folman, R. Probing the origins of inhomogeneous broadening in nitrogen-vacancy centers with Doppler-free-type spectroscopy. *Phys. Rev. B: Condens. Matter Mater. Phys.* **2018**, *98*, 014112.

(21) Davydov, V. A.; Rakhmanina, A. V.; Lyapin, S. G.; Ilichev, I. D.; Boldyrev, K. N.; Shiryaev, A. A.; Agafonov, V. N. Production of nano- and microdiamonds with Si-V and N-V luminescent centers at high pressures in systems based on mixtures of hydrocarbon and fluorocarbon compounds. *JETP Lett.* **2014**, *99*, 585−589.

(22) Basso, L.; Gorrini, F.; Cazzanelli, M.; Bazzanella, N.; Bifone, A.; Miotello, A. An all-optical single-step process for production of nanometric-sized fluorescent diamonds. *Nanoscale* **2018**, *10*, 5738−5744.

(23) Khachatryan, A. K.; Aloyan, S. G.; May, P. W.; Sargsyan, R.; Khachatryan, V. A.; Baghdasaryan, V. S. Graphite-to-diamond transformation induced by ultrasound cavitation. *Diamond Relat. Mater.* **2008**, *17*, 931−936.

(24) Tegetmeyer, B.; Lewes-Malandrakis, G.; Wernet, M.; Schreyvogel, C.; Lang, N.; Yoshikawa, T.; Nebel, C. E. Incorporation of SiV-centers in diamond nanoparticles using silicon background doping. *Diamond Relat. Mater.* **2016**, *65*, 87−90.

(25) Nicolas, L.; Delord, T.; Huillery, P.; Neu, E.; Hétet, G. Diamond nano-pyramids with narrow linewidth SiV centers for quantum technologies. *AIP Adv.* **2018**, *8*, 065102.

(26) Neu, E.; Steinmetz, D.; Riedrich-Möller, J.; Gsell, S.; Fischer, M.; Schreck, M.; Becher, C. Single photon emission from silicon-vacancy colour centres in chemical vapour deposition nano-diamonds on iridium. *New J. Phys.* **2011**, *13*, 025012.

(27) Mahfouz, R.; Floyd, D. L.; Peng, W.; Choy, J. T.; Loncar, M.; Bakr, O. M. Size-controlled fluorescent nanodiamonds: a facile

DOI: 10.1021/acsanm.9b01395
ACS Appl. Nano Mater. XXXX, XXX, XXX−XXX

method of fabrication and color-center counting. *Nanoscale* **2013**, *5*, 11776−11782.
(28) Nistor, L.; Ralchenko, V.; Vlasov, I.; Khomich, A.; Khmelnitskii, R.; Potapov, P.; Van Landuyt, J. Formation of Amorphous Carbon and Graphite in CVD Diamond upon Annealing: A HREM, EELS, Raman and Optical Study. *Physica status solidi (a)* **2001**, *186*, 207−214.
(29) Osswald, S.; Yushin, G.; Mochalin, V.; Kucheyev, S. O.; Gogotsi, Y. Control of sp2/sp3 Carbon Ratio and Surface Chemistry of Nanodiamond Powders by Selective Oxidation in Air. *J. Am. Chem. Soc.* **2006**, *128*, 11635−11642.
(30) Kumar, A.; Ann Lin, P.; Xue, A.; Hao, B.; Khin Yap, Y.; Sankaran, R. M. Formation of nanodiamonds at near-ambient conditions via microplasma dissociation of ethanol vapour. *Nat. Commun.* **2013**, *4*, 2618.
(31) Ferrari, A. C.; Robertson, J. Origin of the 1150 cm^{-1} Raman mode in nanocrystalline diamond. *Phys. Rev. B: Condens. Matter Mater. Phys.* **2001**, *63*, 121405.
(32) Ferrari, A. C.; Robertson, J. Raman spectroscopy of amorphous, nanostructured, diamond−like carbon, and nanodiamond. *Philos. Trans. R. Soc., A* **2004**, *362*, 2477−2512.
(33) Markham, M. L.; Dodson, J. M.; Scarsbrook, G. A.; Twitchen, D. J.; Balasubramanian, G.; Jelezko, F.; Wrachtrup, J. CVD diamond for spintronics. *Diamond Relat. Mater.* **2011**, *20*, 134−139.
(34) Manson, N. B.; Hedges, M.; Barson, M. S. J.; Ahlefeldt, R.; Doherty, M. W.; Abe, H.; Ohshima, T.; Sellars, M. J. NV–N+ pair centre in 1b diamond. *New J. Phys.* **2018**, *20*, 113037.
(35) Zaïtsev, A. M. *Optical Properties of Diamond: A Data Handbook*; Springer: 2001.
(36) Tallaire, A.; Collins, A. T.; Charles, D.; Achard, J.; Sussmann, R.; Gicquel, A.; Newton, M. E.; Edmonds, A. M.; Cruddace, R. J. Characterisation of high-quality thick single-crystal diamond grown by CVD with a low nitrogen addition. *Diamond Relat. Mater.* **2006**, *15*, 1700−1707.
(37) Doherty, M. W.; Manson, N. B.; Delaney, P.; Jelezko, F.; Wrachtrup, J.; Hollenberg, L. C. L. The nitrogen-vacancy colour centre in diamond. *Phys. Rep.* **2013**, *528*, 1−45.
(38) Takeuchi, D.; Watanabe, H.; Sawada, H.; Yamanaka, S.; Ichinose, H.; Sekiguchi, T.; Okushi, H. Origin of band-A emission in homoepitaxial diamond films. *Diamond Relat. Mater.* **2001**, *10*, 526−530.
(39) Boudou, J.-P.; Curmi, P. A.; Jelezko, F.; Wrachtrup, J.; Aubert, P.; Sennour, M.; Balasubramanian, G.; Reuter, R.; Thorel, A.; Gaffet, E. High yield fabrication of fluorescent nanodiamonds. *Nanotechnology* **2009**, *20*, 235602.
(40) Baranov, P. G.; Soltamova, A. A.; Tolmachev, D. O.; Romanov, N. G.; Babunts, R. A.; Shakhov, F. M.; Kidalov, S. V.; Vul', A. Y.; Mamin, G. V.; Orlinskii, S. B.; Silkin, N. I. Enormously High Concentrations of Fluorescent Nitrogen-Vacancy Centers Fabricated by Sintering of Detonation Nanodiamonds. *Small* **2011**, *7*, 1533−1537.
(41) Shames, A. I.; Smirnov, A. I.; Milikisiyants, S.; Danilov, E. O.; Nunn, N.; McGuire, G.; Torelli, M. D.; Shenderova, O. Fluence-Dependent Evolution of Paramagnetic Triplet Centers in e-Beam Irradiated Microcrystalline Ib Type HPHT Diamond. *J. Phys. Chem. C* **2017**, *121*, 22335−22346.
(42) Collins, A. T. Optical centres produced in diamond by radiation damage. *New Diamond Front. Carbon Technol.* **2007**, *17*, 47−61.
(43) Steeds, J. W.; Kohn, S. Annealing of electron radiation damage in a wide range of Ib and IIa diamond samples. *Diamond Relat. Mater.* **2014**, *50*, 110−122.
(44) Forneris, J.; Tengattini, A.; Tchernij, S. D.; Picollo, F.; Battiato, A.; Traina, P.; Degiovanni, I. P.; Moreva, E.; Brida, G.; Grilj, V.; Skukan, N.; Jakšić, M.; Genovese, M.; Olivero, P. Creation and characterization of He-related color centers in diamond. *J. Lumin.* **2016**, *179*, 59−63.
(45) Pezzagna, S.; Rogalla, D.; Wildanger, D.; Meijer, J.; Zaitsev, A. Creation and nature of optical centres in diamond for single-photon emission: overview and critical remarks. *New J. Phys.* **2011**, *13* (3), 035024.
(46) Wee, T.-L.; Tzeng, Y.-K.; Han, C.-C.; Chang, H.-C.; Fann, W.; Hsu, J.-H.; Chen, K.-M.; Yu, Y.-C. Two-photon Excited Fluorescence of Nitrogen-Vacancy Centers in Proton-Irradiated Type Ib Diamond. *J. Phys. Chem. A* **2007**, *111* (38), 9379−9386.
(47) Lühmann, T.; Raatz, N.; John, R.; Lesik, M.; Rodiger, J.; Portail, M.; Wildanger, D.; Kleißler, F.; Nordlund, K.; Zaitsev, A.; Roch, J.-F.; Tallaire, A.; Meijer, J.; Pezzagna, S. Screening and engineering of colour centres in diamond. *J. Phys. D: Appl. Phys.* **2018**, *51*, 483002.
(48) Rondin, L.; Dantelle, G.; Slablab, A.; Grosshans, F.; Treussart, F.; Bergonzo, P.; Perruchas, S.; Gacoin, T.; Chaigneau, M.; Chang, H. C.; Jacques, V.; Roch, J. F. Surface-induced charge state conversion of nitrogen-vacancy defects in nanodiamonds. *Phys. Rev. B: Condens. Matter Mater. Phys.* **2010**, *82*, 115449.
(49) Smith, B. R.; Gruber, D.; Plakhotnik, T. The effects of surface oxidation on luminescence of nano diamonds. *Diamond Relat. Mater.* **2010**, *19* (4), 314−318.
(50) Reineck, P.; Capelli, M.; Lau, D. W. M.; Jeske, J.; Field, M. R.; Ohshima, T.; Greentree, A. D.; Gibson, B. C. Bright and photostable nitrogen-vacancy fluorescence from unprocessed detonation nanodiamond. *Nanoscale* **2017**, *9* (2), 497−502.
(51) Shames, A. I.; Osipov, V. Y.; von Bardeleben, H.-J.; Boudou, J.-P.; Treussart, F.; Vul', A. Y. Native and induced triplet nitrogen-vacancy centers in nano- and micro-diamonds: Half-field electron paramagnetic resonance fingerprint. *Appl. Phys. Lett.* **2014**, *104*, 063107.
(52) Cox, A.; Newton, M. E.; Baker, J. M. 13 C, 14 and 15 N ENDOR measurements on the single substitutional nitrogen centre (P1) in diamond. *J. Phys.: Condens. Matter* **1994**, *6*, 551.
(53) Shames, A. I.; Osipov, V. Y.; Boudou, J. P.; Panich, A. M.; von Bardeleben, H. J.; Treussart, F.; Vul', A. Y. Magnetic resonance tracking of fluorescent nanodiamond fabrication. *J. Phys. D: Appl. Phys.* **2015**, *48*, 155302.
(54) Osipov, V. Y.; Shakhov, F. M.; Efimov, N. N.; Minin, V. V.; Kidalov, S. V.; Vul', A. Y. Identification of paramagnetic nitrogen centers (P1) in diamond crystallites synthesized via the sintering of detonation nanodiamonds at high pressure and temperature. *Phys. Solid State* **2017**, *59*, 1146−1153.
(55) Zhou, X.; Watkins, G. D.; McNamara, K. M.; Messmer, R. P.; Chawla, S. Hydrogen-related defects in polycrystalline CVD diamond. *Phys. Rev. B: Condens. Matter Mater. Phys.* **1996**, *54*, 7881−7890.
(56) Holder, S. L.; Rowan, L. G.; Krebs, J. J. Electron paramagnetic resonance forbidden transitions from hydrogen in polycrystalline diamond films. *Appl. Phys. Lett.* **1994**, *64*, 1091−1093.
(57) Talbot-Ponsonby, D. F.; Newton, M. E.; Baker, J. M.; Scarsbrook, G. A.; Sussmann, R. S.; Whitehead, A. J. EPR and optical studies on polycrystalline diamond films grown by chemical vapor deposition and annealed between 1100 and 1900 K. *Phys. Rev. B: Condens. Matter Mater. Phys.* **1998**, *57*, 2302−2309.
(58) Mizuochi, N.; Watanabe, H.; Isoya, J.; Okushi, H.; Yamasaki, S. Hydrogen-related defects in single crystalline CVD homoepitaxial diamond film studied by EPR. *Diamond Relat. Mater.* **2004**, *13*, 765−768.
(59) Shames, A. I.; Panich, A. M.; Kempinski, W.; Alexenskii, A. E.; Baidakova, M. V.; Dideikin, A. T.; Osipov, V. Y.; Siklitski, V. I.; Osawa, E.; Ozawa, M.; Vul', A. Y. Defects and impurities in nanodiamonds: EPR, NMR and TEM study. *J. Phys. Chem. Solids* **2002**, *63*, 1993−2001.
(60) Hassouni, K.; Silva, F.; Gicquel, A. Modelling of diamond deposition microwave cavity generated plasmas. *J. Phys. D: Appl. Phys.* **2010**, *43*, 153001.
(61) Tsugawa, K.; Ishihara, M.; Kim, J.; Koga, Y.; Hasegawa, M. Nanocrystalline diamond film growth on plastic substrates at temperatures below 100°C from low-temperature plasma. *Phys. Rev. B: Condens. Matter Mater. Phys.* **2010**, *82* (12), 125460.
(62) Kumar, A.; Ann Lin, P.; Xue, A.; Hao, B.; Khin Yap, Y.; Sankaran, R. M. Formation of nanodiamonds at near-ambient

DOI: 10.1021/acsanm.9b01395
ACS Appl. Nano Mater. XXXX, XXX, XXX−XXX

conditions via microplasma dissociation of ethanol vapour. *Nat. Commun.* **2013**, *4*, 2618.
(63) Vandenbulcke, L.; Gries, T.; Rouzaud, J. N. Nanodiamonds in dusty low-pressure plasmas. *Appl. Phys. Lett.* **2009**, *94*, 044106.
(64) Frenklach, M.; Howard, W.; Huang, D.; Yuan, J.; Spear, K. E.; Koba, R. Induced nucleation of diamond powder. *Appl. Phys. Lett.* **1991**, *59* (5), 546−548.
(65) Achard, J.; Silva, F.; Brinza, O.; Tallaire, A.; Gicquel, A. Coupled effect of nitrogen addition and surface temperature on the morphology and the kinetics of thick CVD diamond single crystals. *Diamond Relat. Mater.* **2007**, *16*, 685−689.
(66) Sotoma, S.; Terada, D.; Segawa, T. F.; Igarashi, R.; Harada, Y.; Shirakawa, M. Enrichment of ODMR-active nitrogen-vacancy centres in five-nanometre-sized detonation-synthesized nanodiamonds: Nanoprobes for temperature, angle and position. *Sci. Rep.* **2018**, *8*, 5463.
(67) Williams, O. A.; Hees, J.; Dieker, C.; Jäger, W.; Kirste, L.; Nebel, C. E. Size-Dependent Reactivity of Diamond Nanoparticles. *ACS Nano* **2010**, *4*, 4824−4830.
(68) Arnault, J. C.; Girard, H. A. Hydrogenated nanodiamonds: Synthesis and surface properties. *Curr. Opin. Solid State Mater. Sci.* **2017**, *21*, 10−16.

DOI: 10.1021/acsanm.9b01395
ACS Appl. Nano Mater. XXXX, XXX, XXX−XXX